Наносистеми, наноматеріали, нанотехнології
Nanosistemi, Nanomateriali, Nanotehnologii
2026, т. 24, № 1, сс. 165–174
https://doi.org/10.15407/nnn.24.01.0165

PACS numbers: 61.05.cp, 68.37.Vj, 75.50-y, 81.30.Mh

Preparation and Investigation of Structural Properties of Nano-Spinel Ferrite by Co-Precipitation Method

Leal Abdullah Hamza and Sameer H. Al-Nesrawy

College of Education for Pure Science,
Department of Physics,
University of Babylon,
Hilla, Iraq

The co-precipitation method is used in this study to prepare and characterize the structural properties of two types of ferrites: zinc–nickel ferrite Zn–Ni Fe_2O_4 and zinc–chromium ferrite Zn–Cr Fe_2O_4. These ferrites are separated into two parts: one without sintering and the other after sintering at 1100°C for 3 hours to facilitate further crystallization. The ferrites are investigated by x-ray diffraction (XRD) to confirm Zn–Cr-, Zn–Ni-nanoferrite samples without sintering and sintered at 1100°C. These are attributed to the face-centred cubic (f.c.c.) spinel phase, and the Debye–Scherrer equation is used to determine the average crystallite sizes of the prepared samples, which are found to be equal to 7.05 nm for Zn–Cr-ferrite nanoparticles without sintering and 64.67 nm Zn–Cr-ferrite nanoparticles sintered at 1100°C. Being equal 46.86 nm Zn–Ni-ferrite nanoparticle without sintering and 57.41 nm for the Zn–Ni-ferrite nanoparticle sintered at 1100°C, it is shown that these materials are of nanoscale. The composition of the ferrite has better crystallization. That is sintering at that temperature has led to an increase in the degree of crystallization and a decrease in the crystal defects formed in the ferrites during preparation. The field-emission scanning electron microscope (FE–SEM) is used to examine Zn–Cr-, Zn–Ni-nanoferrite samples without sintering and sintered at 1100°C. The pores separating the particles are eliminated during the sintering process that produces strong bonds in the agglomeration form.

У цьому дослідженні використано метод спільного осадження для одержання та характеризації структурних властивостей двох типів феритів: цинк-ніклевого фериту Zn–Ni Fe_2O_4 та цинк-хромового фериту Zn–Cr Fe_2O_4. Ферити розділено на дві частини: одну без спікання, а іншу після спікання за 1100°C впродовж 3 годин для полегшення подальшої кристалізації. Ферити досліджено за допомогою рентґенівської дифракції для підтвердження зразків наноферитів Zn–Cr, Zn–Ni без спікання

та спечених за 1100°C. Це пояснюється гранецентрованою кубічною шпінельною фазою, і для визначення середніх розмірів кристалітів підготовлених зразків було використано рівняння Дебая–Шеррера, яке дорівнюють 7,05 нм для наночастинок фериту Zn–Cr без спікання та 64,67 нм для наночастинок фериту Zn–Cr, спечених за 1100°C. Дорівнюючи 46,86 нм для наночастинок фериту Zn–Ni без спікання та 57,41 нм для наночастинок фериту Zn–Ni, спечених за 1100°C, ці розміри показують наномасштабність цих матеріялів. Склад фериту має ліпшу кристалізацію, тобто спікання за цієї температури приводить до збільшення ступеня кристалізації та зменшення кристалічних дефектів, що утворюються у феритах під час приготування. Для дослідження зразків наноферитів Zn–Cr, Zn–Ni без спікання та спечених за 1100°C було використано сканувальний електронний мікроскоп з польовою емісією. Пори, що розділяють частинки, були усунені під час процесу спікання, що привело до утворення міцних зв'язків у формі аґломерації.

Key words: co-precipitation, ferrite, nanoparticles, spinel, field-emission scanning electron microscopy, x-ray diffraction.

Ключові слова: співосадження, ферит, наночастинки, шпінель, сканувальна електронна мікроскопія з польовою емісією, рентґенівська дифракція.

(Received 15 September, 2024; in revised form, 17 September, 2024)

1. INTRODUCTION

In science research, magnetic nanoparticle systems have generated great interest, especially in physics and related fields. Owing to their many and significant characteristics, recent advanced research has shifted to the synthesis of metallic oxide nanoparticles, where a pressing need has arisen to produce materials known as nanomaterials-materials with a large surface area relative to their size [1]. Magnetic drug targets, magnetic resonance imaging for medical diagnosis, recording materials and catalysts, environments, and more are just a few of the numerous applications for magnetic nanoparticles [2]. Over time, ferrites have continued to garner interest. Because ferrites are stable, reasonably priced, and have a broad range of technological applications, they cannot be replaced by any other magnetic material [3].

Ceramic materials known as ferrites are created by chemically adding one or more metals to iron oxides (Fe_2O_4). Ferrites are mixtures of two metallic oxides, which can include any bivalent element, such as barium (Ba), zinc (Zn), nickel (Ni), manganese (Mn), or zinc oxide. Ferrites have exceptional magnetic and electrical properties [4]. Based on their structural characteristics, ferrites are divided into two groups: cubic and hexagonal. Soft ferrites are an-

other name for cubic ferrites.

These cubic ferrites are further classified into two types: spinel ferrite and garnet ferrite. Hexagonal ferrites are also known as hexaferrites and are hard ferrites because it is tough to magnetize and demagnetize them. They are also known as permanent [5]. Applications for hard ferrites include microwave absorbing systems, refrigerators, loudspeakers, washing machines, TVs, communication systems, switch-mode power supplies, and high-frequency applications. However, soft ferries have a wide range of uses in the electronic industry, including the development of transformer cores, high-frequency inductors, and microwave components, due to their good magnetic field conductivity [6].

Soft chemical techniques like hydrothermal synthesis, sol–gel, and co-precipitation can be used to create ferrite particles at the nanoscale [7]. Because co-precipitation does not require high pressure or temperature and because impure materials are removed through filtration and washing, it is an appropriate chemical method for synthesizing nanoparticles [8]. The benefits of the co-precipitation method include high yield, high purity of product, and ease of use [9]. From a physical perspective, the co-precipitation process is driven by three main mechanisms: Surface adsorption: Ions in solution with the opposing charge can be drawn to the precipitate's surface charge. Inclusion: The analyte can high frequency be incorporated non-isomorphically (solid solution) or isomorphically (mixed crystal) to replace an ion in the precipitate's crystal structure. Additionally, Ions are physically engulfed in the precipitate before they can diffuse or disperse, known as occlusion [10].

2. EXPERIMENTAL

Synthesis of the ferrite nanoparticles was done by co-precipitation in two parts: part one, was mixed thoroughly 8.11 gm ferric chloride $FeCl_3$, 11.9 gm chrome nitrate $Cr(NO_3)\cdot 9H_2O$ and 14.85 gm zinc nitrate $Zn(NO_3)_2$ and part two, 8.11 gm ferric chloride $FeCl_3$, 14.54 gm nickel nitrate $Ni(NO_3)_2$ and 14.85 gm zinc nitrate $Zn(NO_3)_2$ as starting materials, each starting material was weighted separately and add 100 ml of distilled water and then mixed all these cationic solutions while stirring to complete dissolution. A sufficient amount of the NaOH solution is made at a concentration of 2M. After that, a thin stream of NaOH solution is added to the cationic solution while stirring and heating the mixture until precipitation happens. To finish the reaction, the precipitate is heated to a temperature of 50°C while still in its alkaline state. After another hour of stirring to allow the particles to age, the precipitated particles are filtered and repeatedly cleaned before being dried for an hour at 150 degrees Cel-

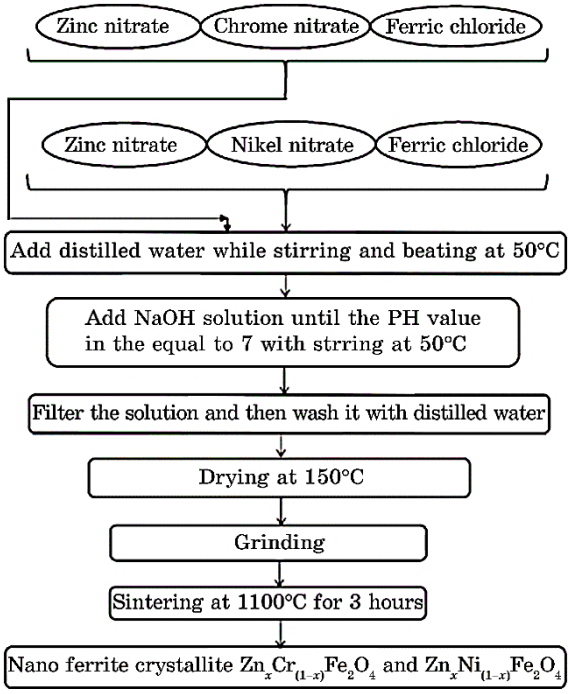

Fig. 1. Preparation steps of nanoferrite crystallite.

sius.

After that, the co-precipitated ferrite agglomerates were ground into extremely fine particles for a few minutes using an agate mortar and pestle. These particles are finally sintering at 1100 degrees Celsius to continue crystallizing. The primary steps used in the preparation are schematically represented in Fig. 1.

3. RESULTS AND DISCUSSION

3.1 XRD Analysis and Particle Size Calculation

Figures 2, 3 show the XRD pattern of the Zn–Cr Fe_2O_4 nanoparticle prepared using co-precipitation technique.

Figure 2 the sample without sintered, the appearance of some phases shows the part of the oxides of raw materials at $\theta = 29.3$, 31.9, 38.9, 47.9 because the Zn–Cr ferrite phase isn't grown yet, at $\theta = 35.1$ which there is a partial phase grown of Zn–Cr ferrite.

Figure 3 sintered at 1100°C for 3 hours, x-ray diffraction pattern shows fully the growth of crystalline Zn–Cr ferrites phases. Different peaks appear on the XRD pattern, namely, $2\theta = 30.09$, 35.42,

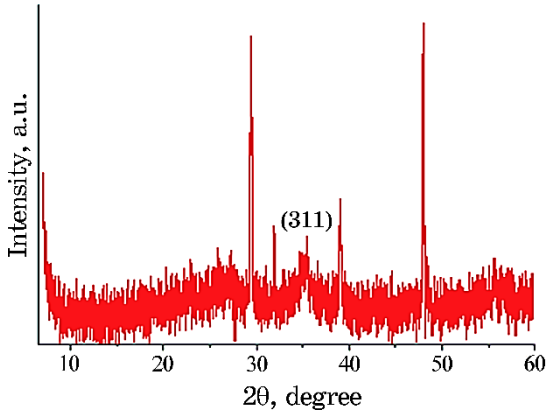

Fig. 2. The XRD pattern of the Zn–Cr ferrite nanoparticle without sintered.

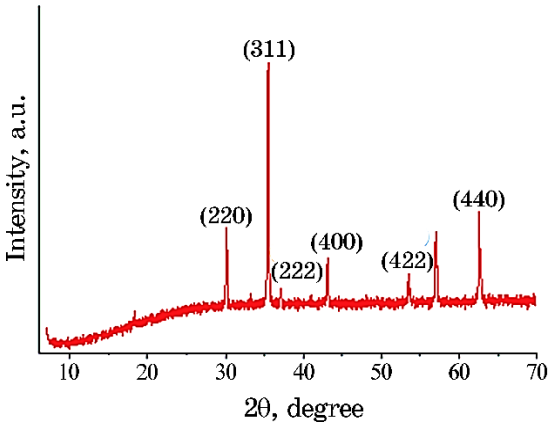

Fig. 3. The XRD pattern of the Zn–Cr ferrite nanoparticle sintered at 1100°C.

37.05, 43.05, 53.39, and 62.51 degrees, which are attributed to (220), (311), (222), (400), (422), (511) and (440) planes, respectively. The pattern of Zn–Cr ferrite nanoparticles is compatible with (JCPDS card numbers 84-0314 and 89-1012). Verification of the face-centred cubic spinel phase (FCC) [11]. The Debye-Scherer's equation has been used to determine the average crystallite size:

$$D = 0.9\lambda/(\beta\cos\theta_\beta), \quad (1)$$

where λ is the incident x-ray radiation wavelength 1.54056 Å, β is the peak's full width at half maximum (radian), and (θ_β) is the XRD

TABLE 1. The XRD result obtained for the Zn–Cr ferrite nanoparticle without sintered.

Component	2θ, degree	*hkl*	*FWHM*, β, degree	*d*, Å	Crystallite size, nm	Average crystallite size, nm
Zn–Cr·Fe_2O_4	35.13	311	1.2343	2.56683	7.054478	7.054478

TABLE 2. The XRD result obtained for the Zn–Cr ferrite nanoparticle sintered at 1100°C.

Component	2θ, degree	*hkl*	*FWHM*, β, degree	*d*, Å	Crystallite size, nm	Average crystallite size, nm
Zn–Cr·Fe_2O_4	30.09	220	0.1511	2.96835	56.88784	64.67817408
	35.42	311	0.1448	2.53081	60.18393	
	37.05	222	0.1278	2.42308	68.50793	
	43.05	400	0.1329	2.09797	67.15018	
	53.39	422	0.1328	1.71284	69.98047	
	62.51	440	0.1486	1.4834	65.35871	

peak's Bragg diffraction angle (degree) [12]. Tables 1 and 2 provide the assignments of different reflections as well as a detailed analysis of the XRD.

Figures 4 and 5 show the XRD pattern of the Zn–Ni Fe_2O_4 nanoparticle prepared too using the co-precipitation technique.

Figure 4 shows the diffraction pattern of ferrite without sintered and Fig. 5 shows the X-ray diffraction pattern of the same nanoferrite using sintering at a temperature of 1100°C for 3 hours. When comparing these patterns, Fig. 4 shows that the dominant direction (311) also remains for the sintered ferrite, with its intensity increasing with sintering at the expense of other peaks. This indicates the presence of some levels that are preferred for the growth of crystalline directions, and the intensity of this peak increases accordingly, which confirms that the ferrite composition has better crystallization. That is, sintering at that temperature has led to an increase in the degree of crystallization and a decrease in the crystalline defects formed in the ferrite during preparation, which indicates that sintering leads to a rise in crystalline regularity.

The diffraction patterns match the spinel ferrite standard pattern (ICDD no. 00-022-1012) fairly well. At diffraction angles (2θ) of 29.9, 35.3, 36.9, 42.8, 53.1, 56.6, 62.2, 70.5, 73.5, and 74.5 degrees, they are clearly defined and comprise robust reflection peaks that are attributed to the (220), (311), (222), (400), (422), (511), (440), (620), (533), and (622) planes, respectively. By taking into

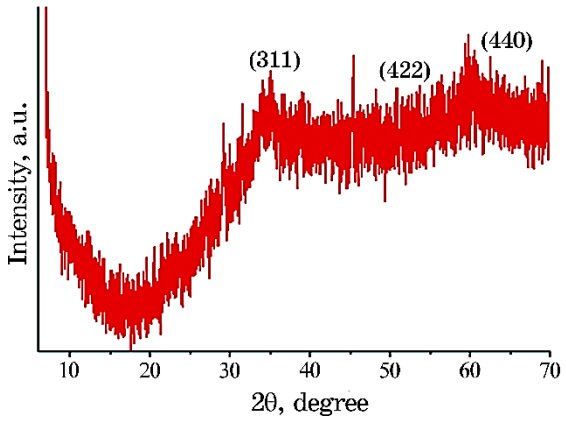

Fig. 4. The XRD pattern of the Zn–Ni ferrite nanoparticle without sintered.

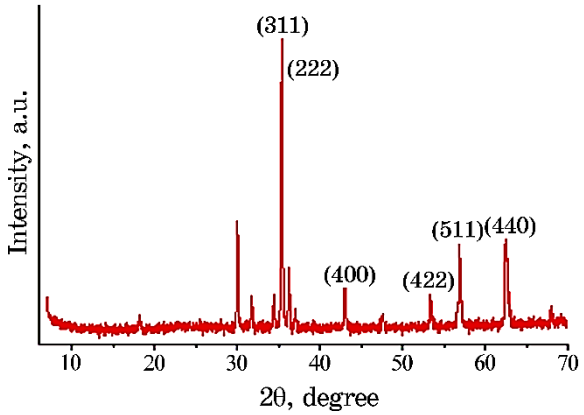

Fig. 5. The XRD pattern of the Zn–Ni ferrite nanoparticle sintered at 1100°C.

account the strongest diffraction peaks in XRD spectra, the crystal size of the ferrite samples was ascertained [13]. In this study, the crystal size of the tested sample was determined. The crystal size of the ferrite samples was ascertained by taking into account the strongest diffraction peaks in XRD spectra using Scherrer's formula, as indicated in Eq. (1). Tables 3, 4 are a summary of the crystallite size D calculation.

3.2. Field-Emission–Scanning Electron Microscopy (FE–SEM)

FE–SEM was used to examine Zn–Cr Nano ferrite samples without

TABLE 3. The XRD result obtained for the Zn–Ni ferrite nanoparticle without sintered.

Component	2θ, degree	*hkl*	*FWHM*, degree	*d*, Å	Crystallite size, nm	Average crystallite size, nm
Zn–Ni·Fe_2O_4	35.3	311	0.9323	3.06377	9.199623	46.86716588
	53.1	422	6.0734	2.56683	1.43285	
	62.2	440	0.0692	2.0012	129.969	

TABLE 4. The XRD result obtained for the Zn–Ni ferrite nanoparticle sintered at 1100°C.

Component	2θ, degree	*hkl*	*FWHM*, degree	*d*, Å	Crystallite size, nm	Average crystallite size, nm
Zn–Ni Fe_2O_4	35.3609	311	0.1554	2.53632	56.0663222	57.41132041
	36.2246	222	0.1321	2.4778	66.1159439	
	42.9799	400	0.1687	2.1027	52.8816646	
	53.3301	422	0.1692	1.71645	54.8963699	
	56.5681	511	0.1313	1.62564	71.7883791	
	62.4414	440	0.2272	1.4861	42.7192428	

sintered and sintered at 1100°C for 3 hours.

Figure 6, *a*, *b* depicts a typical FE–SEM image. The FE–SEM image *b* is nearly uniform and agglomerated grains are observed [11]. Particle aggregation takes place in the nanometer range, as seen in FE–SEM image *b*. As seen in image a, the pores separating the particles were eliminated during the sintering process, which produced strong bonds in the agglomeration form. The limited grain size of the particle is determined by the interplay between porosity and the grain boundary. Through this investigation, it was found that when the particles were sintered at 1100°C, their average grain size decreased.

Figure 7, *a*, *b* shows FE–SEM pictures of Zn–Ni Fe_2O_4 NPs. The FE–SEM images of the zinc-nickel ferrite without sintered and sintered at 1100°C for 3 hours.

Figure 7, *a* without sintered shows irregular, non-symmetrical particles. For the Zn–Ni ferrite sample sintered at 1100°C, Fig. 7, *b* the agglomeration shows uniform particles [14]. The FE–SEM image shows that the agglomeration of Zn–Ni ferrite that sintered at 1100°C nanoparticle is relatively higher when compared to that of the without sintered nanoparticles because of the effect of the capping agent on modifying crystal sizes.

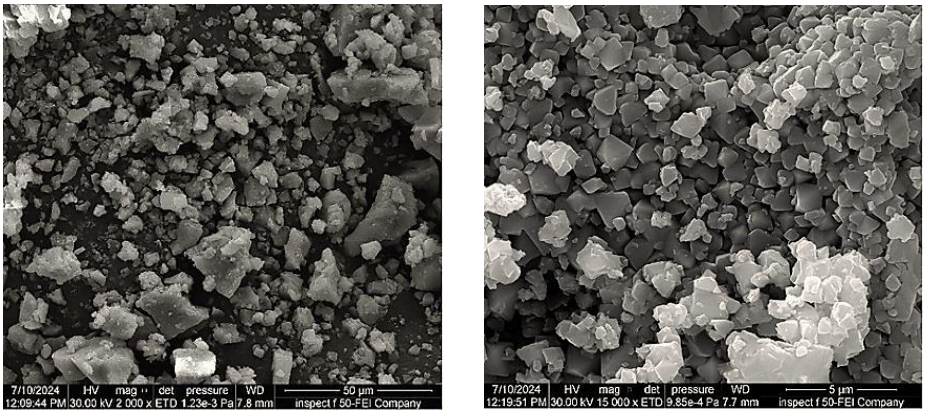

a *b*

Fig. 6. FE–SEM images for Zn–Cr ferrite: (*a*) without sintered; (*b*) sintered at 1100°C.

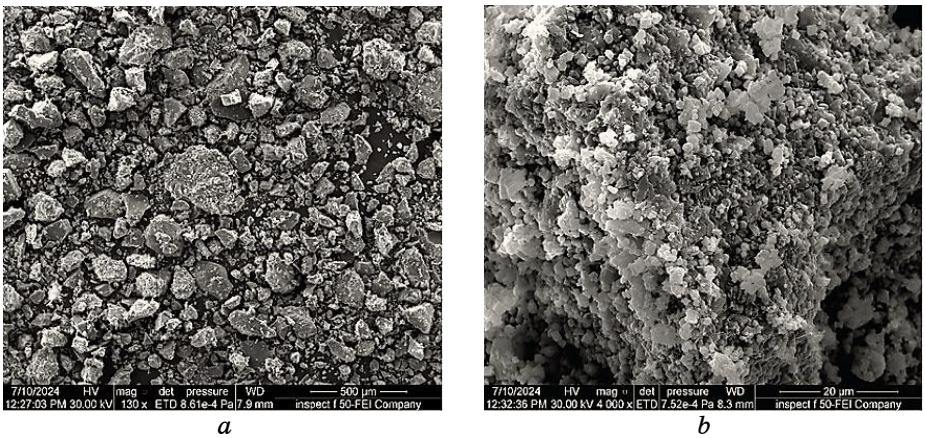

a *b*

Fig. 7. FE–SEM images for Zn–Ni ferrite: (*a*) without sintered; (*b*) sintered at 1100°C.

4. CONCLUSION

In conclusion, this study found the following:
1. the powders obtained by co-precipitated presented the formation of Zn–Cr ferrite and Zn–Ni ferrite crystalline phase;
2. the powders' crystallinity and crystallite size increased with sintered at 1100°C for 3 hours in the spinel lattice Zn–Cr ferrite and Zn–Ni ferrite;
3. all the compositions studied here by means of the XRD and FE–SEM showed the formation of soft nanoparticles' agglomerates.

REFERENCES

1. W. A. Shatti, Z. M. A. Abbas, and Z. T. Khodair, *Journal of Ovonic Research*, **18**, No. 4: 473 (2022); https://doi.org/10.15251/JOR.2022.184.473
2. P. L. Hariani, M. Faizal, Ridwan, Marsi, and D. Setiabudidaya, *International Journal of Environmental Science and Development*, **4**, No. 3: 336 (2013); https://doi.org/10.7763/IJESD.2013.V4.366
3. S. V. Soni, C. L. Khobragade, R. K. Khatarkar, and U. V. Rathod, *Archives of Physics Research*, **5**, No. 6: 49 (2014).
4. A. Vedrtnam, K. Kalauni, S. Dubey, and A. Kumar, *AIMS Materials Science*, **7**, No. 6: 800 (2020); https://doi.org/10.3934/matersci.2020.6.800
5. A. Sharma, H. Mahajan, I. Mohammed, S.K. Godara, S. Sinha, and A. K. Srivastava, *Materials Performance and Characterization*, **12**, No. 1: 64 (2023); https://doi.org/10.1520/MPC20220084
6. P. Thakur, S. Taneja, D. Chahar, N. Bhalla, and A. Thakur, *Ceramics International*, **46**, No. 10: 15740 (2020); https://doi.org/10.1016/j.ceramint.2020.03.287
7. B. P. Rao, A. M. Kumar, K. H. Rao, Y. L. N. Murthy, O. F. Caltun, I. Dumitru, and L. Spinu, *Journal of Optoelectronics and Advanced Materials*, **8**, No. 5: 1703 (2006).
8. S. Tazikeh, A. Akbari, A. Talebi, and E. Talebi, *Materials Science—Poland*, **32**, No. 1: 98 (2014); https://doi.org/10.2478/s13536-013-0164-y
9. D. D. Kulkarni, V. R. Joshi, S. N. Shetty, S. B. Patel, and M. S. Khalfe, *IJARSCT*, **2**: 2581 (2022); https://doi.org/10.48175/IJARSCT-3467
10. N. Bader, A. A. Benkhayal, and B. Zimmermann, *Int. J. Chem. Sci.*, **12**, No. 2: 519 (2014).
11. R. R. Powar, V. D. Phadtare, V. G. Parale, S. Pathak, P. B. Piste, and D. N. Zambare, *Journal of the Korean Ceramic Society*, **56**, No. 5: 474 (2019); https://doi.org/10.4191/kcers.2019.56.5.06
12. A. J. Mohammed and S. H. Al-Nesrawy, *Neuro Quantology*, **20**: 251 (2022); https://doi.org/10.14704/nq.2022.20.3.NQ22087
13. M. Suwan, N. Sangwong, and S. Supothina, *Ceramics–Silikaty*, **64**, No. 2: 172 (2020); https://doi.org/10.13168/cs.2020.0006
14. W. R. M. Alsuiai, B. S. Yadav, A. K. Singh, and V. Singh, *Webology*, **19**, No. 2: 2258 (2022).